Cell

A Phage Tubulin Assembles Dynamic Filaments by an Atypical Mechanism to Center Viral DNA within the Host Cell

James A. Kraemer,[1,3] Marcella L. Erb,[2,3] Christopher A. Waddling,[1] Elizabeth A. Montabana,[1] Elena A. Zehr,[1] Hannah Wang,[2] Katrina Nguyen,[2] Duy Stephen L. Pham,[1,4] David A. Agard,[1,*] and Joe Pogliano[2,*]
[1]Department of Biochemistry and Biophysics and the Howard Hughes Medical Institute, University of California, San Francisco, San Francisco, CA 94158, USA
[2]Division of Biological Sciences, University of California, San Diego, San Diego, CA 92093, USA
[3]These authors contributed equally to this work
[4]Present address: Department of Chemistry and Biochemistry, University of California, Los Angeles, Los Angeles, CA 90095, USA
*Correspondence: agard@msg.ucsf.edu (D.A.A.), jpogliano@ucsd.edu (J.P.)
DOI 10.1016/j.cell.2012.04.034

SUMMARY

Tubulins are essential for the reproduction of many eukaryotic viruses, but historically, bacteriophage were assumed not to require a cytoskeleton. Here, we identify a tubulin-like protein, PhuZ, from bacteriophage 201φ2-1 and show that it forms filaments in vivo and in vitro. The PhuZ structure has a conserved tubulin fold, with an unusual, extended C terminus that we demonstrate to be critical for polymerization in vitro and in vivo. Longitudinal packing in the crystal lattice mimics packing observed by EM of in-vitro-formed filaments, indicating how interactions between the C terminus and the following monomer drive polymerization. PhuZ forms a filamentous array that is required for positioning phage DNA within the bacterial cell. Correct positioning to the cell center and optimal phage reproduction only occur when the PhuZ filament is dynamic. Thus, we show that PhuZ assembles a spindle-like array that functions analogously to the microtubule-based spindles of eukaryotes.

INTRODUCTION

Long thought to be a defining eukaryotic feature, the cytoskeleton is now known to have evolved first in prokaryotes (Cabeen and Jacobs-Wagner, 2010; Michie and Löwe, 2006; Thanbichler and Shapiro, 2008). Prokaryotic actin and tubulin homologs possess low-protein sequence identity to their eukaryotic counterparts; however, the degree of structural homology is quite high. The cell shape determining protein MreB, for example, is structurally similar to actin even though it only shares limited sequence identity within residues that line the nucleotide-binding pocket (Thanbichler and Shapiro, 2008; van den Ent et al., 2001). Since the discovery of MreB, >35 families of actin homologs have been identified that perform a diverse set of functions from forming scaffolds to actively segregating DNA (Derman et al., 2009; Thanbichler and Shapiro, 2008). Despite having similar monomeric structures, many of these actins have evolved unique biochemical properties and form filaments with distinct structural features (Becker et al., 2006; Derman et al., 2009; Polka et al., 2009; Popp et al., 2010; Rivera et al., 2011).

Although it is now clear that a key feature of the bacterial actin cytoskeleton is its remarkable diversity of sequence and function, relatively few families of tubulin-like proteins have been characterized in prokaryotes, raising the question of whether bacterial tubulins are similarly biochemically and structurally diverse. The most widely conserved bacterial tubulin is FtsZ, which is found in nearly all bacteria and many archaea. FtsZ assembles an essential component of the cytokinetic ring required for septation (de Boer, 2010; Löwe and Amos, 2009; Lutkenhaus, 2007; Margolin, 2009). Besides FtsZ, two other families of bacterial tubulin-like proteins (BtubA/BtubB and TubZ) have been characterized. BtubA/BtubB of *Prosthecobacter dejongeii* are closely related to α/β-tubulin, but their functions are currently unknown (Schlieper et al., 2005; Sontag et al., 2005). TubZ actively segregates large, low copy number plasmids of many *Bacillus* species by interaction with the TubR DNA-binding protein and the *tubC* locus (Anand et al., 2008; Larsen et al., 2007; Ni et al., 2010). Structures of TubZ and FtsZ reveal a striking conservation of the tubulin fold even though the degree of primary sequence homology to eukaryotic tubulin is extremely low (<14%) (Aylett et al., 2010; Löwe and Amos, 1998; Ni et al., 2010; Nogales et al., 1998a). Intersubunit longitudinal contacts within filaments have been mostly conserved throughout the tubulin families, whereas other contacts appear to be more divergent (Aylett et al., 2010; Löwe and Amos, 2009).

Here, we report a family of divergent tubulins, named "PhuZ" for *ph*age tu*b*ulin/Fts*Z* encoded within phage genomes. We characterize one member of this family (GP59) from *Pseudomonas chlororaphis* phage 201ϕ2-1 (Thomas et al., 2008).

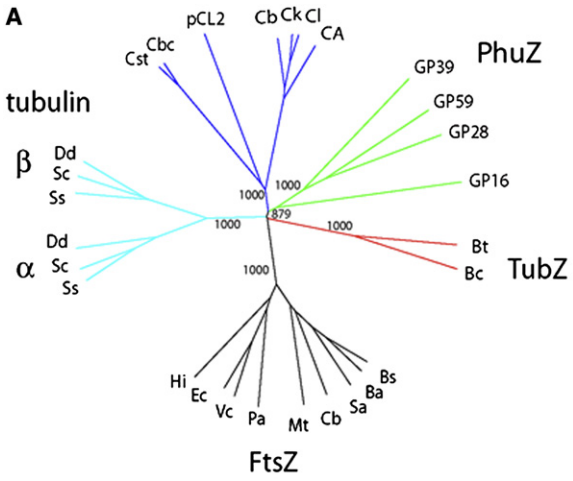

B

		L1	G box
FtsZ	Bs	IGVGGGGNNAV	AGMGGGTGTGAAPVI
	Mt	VGIGGGGVNAV	AGEGGGTGTGGAPVV
	Ec	IGVGGGGGNAV	AGMGGGTGTGAAPVV
TubZ	Bt	IGAGQKGNKEA	LGAGGGVGTGWGSLV
PhuZ	GP59	IFAGGTGMNVA	YSLGGGSGSVLGPLI
	GP39	YFCGGAGFRIG	YSMGGASGSTIGPSL
	GP16	YLMGGAGINIG	ASTAGGTGRVMAMIA
Tub	α Ss	IHVGQAGVQIG	HSFGGGTGSGFTSLL
	β Ss	IQIGQCGNQIG	HSLGGGTGSGMGTLL

C

acidic knuckle

```
GP59 291 QQSKFTQRNPIIDADDNVDEDGMVV 315
GP28 291 AQVRYQQRNAIIDIDDNRTDDGFVV 315
GP39 302 AKANMRKRQSTLDVDDQATSSGLVFD 327
Cb   309 KAARSRKRSVMIDIDDNYEKNEEISIDNFLDEDFQF 344
Ca   309 KQSRDKARSVIIDFDDEGSNNENNSDDTLEFSFE 342
Ck   309 KLSRNKKRSVIIDLDTDSNEKDEELDVLNSNELNNLLEDNYNL 351
Cl   309 KLSRNKKRSVIIDIDTDGIDNKEDIDGLNNSELNDLFEDNYAF 351
              *. ..*.*.
```

Figure 1. Phylogenetic Relationship and Conserved Sequences of PhuZ and Other Distantly Related Tubulins

(A) Phylogenetic tree showing the relationship of divergent tubulins encoded by *Pseudomonas* phage (PhuZ), *Clostridial* sequences from chromosomes (Cb, Ck, Cl, CA), plasmid (pCL2), and phage (Cst, Cbc), and TubZ (pBtoxis/*B.thuringiensis* and pH308197/*B. cereus*) and representative bacterial FtsZ sequences. PhuZ sequences (green) include GP59 (*P. chlororaphis* phage 201ϕ2-1), GP39 (*P. aeruginosa* phage ϕKZ), and GP16 (*P. aeruginosa* phage EL). FtsZ sequences consist of *B. subtilis* (Bs), *B. anthracis* (Ba), *S. aureus* (Sa), *C. botulinum* (Cb), *M. tuberculosis* (Mt), *E. coli* (Ec), *V. cholerae* (Vc), *P. aeruginosa* (Pa), and *H. influenzae* (Hi). *Clostridial* sequences (blue) are CAC3459 *Clostridium acetobutylicum* ATCC824 (CA), CBY3413 *C. butyricum* 5521 (Cb), CKL0570 *C. kluyveri* DSM555 (Ck), Clocel4294 *C. cellulovorans* 743B (Cl), pCLG2A0045 *C. botulinum str.1873* (pCL2), Cst189 *C. botulinum* phage C-st (Cst), and CBCA1765 *C. botulinum C str.* (Cbc). *Eklund*; eukaryotic α/β-tubulin sequences (cyan) include *Dictyostelium discoideum* (Dd), *Saccharomyces cerevisiae* (Sc), and *Sus scrofa* (Ss). Sequences were aligned using Tcoffee, and the tree was generated using ClustalW. Bootstrap values are given for selected branches.

(B) Alignment of L1 and G box motifs for PhuZ, TubZ, α/β-tubulin, and representative bacterial FtsZ sequences. Conserved residues are in red. PhuZ GP59 (phage 201ϕ2-1), GP39 (phage ϕKZ), and GP16 (phage EL), TubZ from pBtoxis, FtsZ sequences (Bs, *B. subtilis*; Mt, *M. tuberculosis*; Ec, *E. coli*) are shown. α/β-Tubulin of *Sus scrofa* (Ss) is indicated.

(C) Alignment of the last 13 amino acids of PhuZ (GP59) that make up the acidic knuckle with PhuZ-related proteins encoded by phage ϕKZ (GP39) and EL (GP16) is presented. Conserved acidic residues are in red.

Isolated from soil samples in 2001, 201ϕ2-1 is one of the largest phage genomes in GenBank at 316 kb. We determined the structure of PhuZ to 1.67 Å resolution and characterized PhuZ polymerization in vivo and in vitro. We show that PhuZ assembles dynamic polymers required for positioning phage DNA at the cell center and that accurate positioning is important for phage reproduction.

RESULTS

Identification of Phage-Encoded Family of Tubulins, PhuZ

We surveyed the genomic database and found a number of tubulin-like protein sequences encoded within several different phage genomes. A phylogenetic tree demonstrates that these phage-encoded tubulins are extraordinarily diverse and are only distantly related to the cell division protein FtsZ and the plasmid segregation protein TubZ (Figures 1A and 1B). All of the phage genomes encoding these tubulins are very large, ranging from 186 to 316 kb, and they infect both Gram-negative and Gram-positive bacteria. Although many of these phage have been characterized previously, no evidence for a tubulin-based cytoskeletal polymer has been reported.

PhuZ Forms Dynamic Filaments In Vivo and In Vitro

To study one of these tubulin-like proteins and determine if it had the ability to polymerize in vivo, we generated a GFP fusion to the *phuZ* gene (*gp59*) from phage 201ϕ2-1 and expressed it from the arabinose promoter (Qiu et al., 2008) on a plasmid in *P. chlororaphis*. When expressed at 30°C at low levels (0.15% or 0.25% arabinose), fluorescence from GFP-PhuZ was uniform throughout the cell (Figure 2A). As the arabinose concentration increased, a threshold concentration (0.4%) was reached where the majority of cells (82%) spontaneously assembled filaments

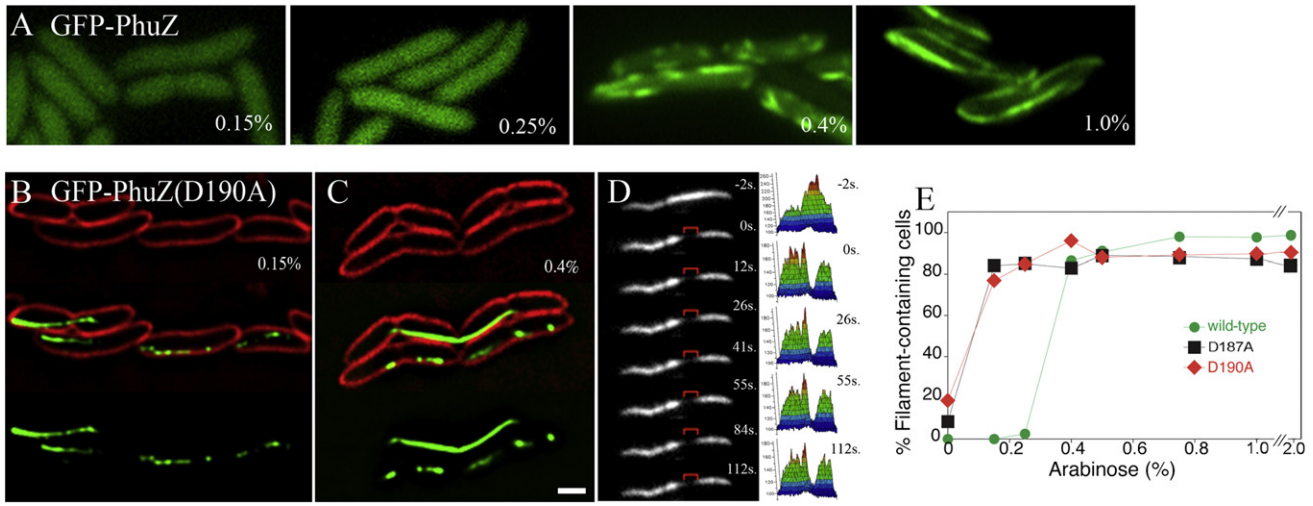

Figure 2. PhuZ Polymer Assembly in *P. chlororaphis*

(A) Fluorescent micrographs of *P. chlororaphis* cells expressing wild-type GFP-PhuZ grown at 30°C and induced with the indicated amount (%) of arabinose are shown. Scale bar, 1 μm.

(B and C) The catalytic point mutant GFP-PhuZD190A forms filaments that become trapped in septa. Membranes are stained red with FM4-64. Scale bar, 1 μm.

(D) Photobleaching of GFP-PhuZD190A is demonstrated. The bleached zone generated at time 0 s (red bracket) does not move or recover after 112 s, indicating that the filaments are static.

(E) Graphs showing the percentage of cells containing filaments when fusion proteins are expressed at increasing levels. Cells were grown at 30°C for wild-type and catalytic point mutants.

See also Figure S1 and Movies S1, S2, and S3.

(Figures 2A and 2E). Quantitation of GFP-PhuZ expression using in-gel fluorescence demonstrated that the fusion protein was full length and that expression increased linearly with arabinose concentration (see Figure S1 available online). When expressed just above the threshold inducer concentration for assembly (0.4%), cells contained multiple filaments (Figure 2A) that moved rapidly throughout the cell (Movie S1). At higher expression levels (1%), GFP-PhuZ filaments extended the entire length of the cell (Figure 2A).

To gain insight into the nature of PhuZ filaments observed in vivo, PhuZ was expressed recombinantly, purified (Figure S2A), and its in vitro polymer growth kinetics examined by right-angle light scattering. As with other tubulins, PhuZ polymerizes in a GTP-dependent manner, with no polymerization observed in the presence of GDP (Figure 3A). It also displays a lag phase characteristic of a nucleation-extension mechanism of polymer growth. As expected, the length of the lag phase and maximum signal at the plateau are proportional to the concentration of PhuZ, from which we determine the critical concentration to be 2.8 ± 0.1 μM (Figure S2B).

To assess the morphology of PhuZ filaments, PhuZ was polymerized in vitro in the presence of the nonhydrolyzable GTP analog GMPCPP and examined by negative-stain electron microscopy (EM). Figure 3C shows a representative micrograph of individual PhuZ filaments together with high-magnification views (also Figure S2). The morphology of PhuZ filaments is distinct from microtubules formed by tubulin and single-stranded filaments formed by FtsZ but is reminiscent of the two-stranded, helical filaments formed by TubZ (Aylett et al., 2010; Chen and Erickson, 2008). Although crossover events are observed in the PhuZ filaments, they appear at irregular intervals, and their architecture is not immediately evident. Further EM analysis will be required to determine the detailed structure of the filaments.

Structure of the PhuZ-GDP Monomer

To better understand the similarities and differences between PhuZ and other tubulins, crystals of wild-type and Se-Met PhuZ were grown in the presence of GDP, and the structure of Se-Met PhuZ was solved by MAD phasing (Table S1) and subsequently refined using the 1.67 Å resolution, wild-type PhuZ-GDP data (Figure 4A). The initial $2F_o$-F_c electron density maps at 1.67 Å showed strong density for GDP in the nucleotide-binding pocket (Figure 4B). As in other tubulins, the structure of PhuZ consists of two domains: an N-terminal domain containing the nucleotide-binding pocket (Figure 4B) and C-terminal domain, bridged by a long, central helix, H7. Notably, a short loop replaces the normally highly conserved tubulin interdomain helix, H6. The structure of PhuZ represents the first tubulin homolog in which all of the C-terminal residues have been observed, revealing that they form an extended C-terminal tail (residues 295–315) appended to a long helix, H11. Overlays of the PhuZ backbone structure with those of α-tubulin (Nogales et al., 1998b), *Aquifex aeolicus* FtsZ (Oliva et al., 2007), and TubZ (Aylett et al., 2010) result in calculated rmsd values of 2.9, 2.6, and 2.9 Å, respectively (Figure S3). The PhuZ structure is too divergent from αβ-tubulin to unambiguously determine if this represents a straight or curved conformation.

Although the tertiary structure of PhuZ is highly consistent with the structure of other tubulin family members, there are several notable differences. As in tubulins, PhuZ lacks the N-terminal extension present in both FtsZ and TubZ. Surprisingly, H6, which

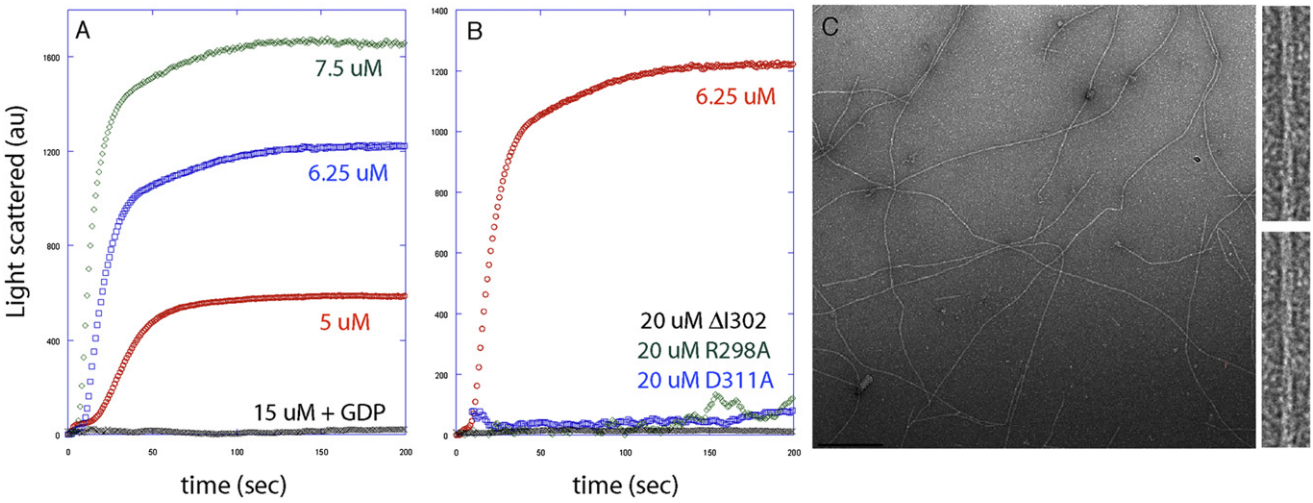

Figure 3. In Vitro Polymerization of PhuZ

(A) Right-angle light-scattering traces of PhuZ polymerization at 5 μM (red), 6.25 μM (blue), and 7.5 μM (green) upon addition of 1 mM GTP are illustrated. Black trace is of 15 μM PhuZ with 1 mM GDP.

(B) Right-angle light-scattering traces of PhuZ mutants at 20 μM (ΔI302, black; R298A, green; D311A; blue) show no detectable polymer formation. The 6.25 μM wild-type trace is shown for comparison.

(C) Negative-stain EM of 7 μM PhuZ polymerized in the presence of 1 mM GMPCPP at 36,000× is presented. Two boxed segments of filaments collected at 52,000× are shown at right to indicate detailed filament.

See also Figure S2.

makes key longitudinal contacts in forming tubulin and FtsZ protofilaments (Downing and Nogales, 1998), is missing in PhuZ. The absence of H6 leaves an acidic surface patch in its place (Figure S3D). The PhuZ C-terminal domain is smaller in size than in other tubulin family members due to smaller loops and helices, especially H10. Like TubZ, PhuZ contains a long helix, H11, after the conserved C-terminal domain (Aylett et al., 2010; Ni et al., 2010).

The Nucleotide-Binding Pocket Is Conserved and Contains Key Catalytic Residues Required for Polymer Dynamics

Within the highly conserved nucleotide-binding pocket (Figures 4A and 4B), backbone nitrogen atoms in loops L1 and L4 coordinate the phosphates. Although the GQxG motif in L1 is conserved across eukaryotic tubulins and TubZ, in PhuZ, L1 contains the sequence 11-GGTG-14, replacing the conserved Gln with a Gly, as in FtsZ (Figure 1B). As a consequence, the L1 loop has a tighter turn leading into H1. How this affects nucleotide binding is unclear. The GGGTGT/SG tubulin consensus sequence, or G box, in L4 is also slightly varied to 91-GGGSGSV-97 in PhuZ (Figure 1B), although the presence of the Val side chain does not appear to affect the conserved structural elements (Figure S3). As expected, the nucleotide base pi stacks with Y161 and hydrogen bonds with N16, N155, and N165 (Figure 4B). Residues S89, E122, N126, and Y161, plus two water molecules, all provide hydrogen-bonding interactions with the sugar. These interactions are consistent with the highly conserved nucleotide-binding mode of other tubulins.

The catalytic loop, T7, which normally inserts itself into the nucleotide-binding pocket of the preceding longitudinal monomer to aid in GTP hydrolysis, is modified from the GxxNxDxxD/E tubulin/FtsZ consensus sequence to NxxRxDxxD, although the key catalytic DxxD residues are conserved. To confirm the functional assignment of these aspartates, they were separately mutated to alanines. Similar mutations in TubZ and FtsZ compromise GTP hydrolysis but not GTP binding, and as a result, the mutant proteins form long static polymers (Larsen et al., 2007; Lu et al., 2001). GFP-PhuZD187A (Figure S4A) and D190A (Figures 2B–2E) mutants were expressed from the arabinose promoter in *P. chlororaphis*. Both of the mutant proteins behaved similarly and were dramatically different from wild-type. When expressed at low arabinose concentrations at 30°C (0.15%), both of the mutant proteins assembled short polymers in approximately 80% of the cells, suggesting that they had a lower threshold concentration for assembly (Figures 2B, 2E, and S3). There was also no detectable accumulation of diffuse fluorescence in the background of the cells, and a significant percentage of cells (10% for D187A and 18% D190A) assembled filaments even when no arabinose was present, suggesting that even the smallest amount of expressed protein assembled polymers (Figures 2E and S3). When expressed at higher levels (0.4% arabinose), both mutants formed long filaments that often chained the cells together (Figure 2C). In contrast to wild-type filaments, the mutant filaments appeared relatively immobile in time-lapse experiments (Movie S2). We used fluorescence recovery after photobleaching (FRAP) to quantitate turnover dynamics within these mutant filaments. Unlike wild-type filaments (Figure S4B), no recovery or movement of the bleached zone over time (Figure 2D; Movie S3) was observed in the mutants, even after extended periods, indicating that the filaments are completely static. These results are consistent with an essential role for these two residues for PhuZ GTP hydrolysis and polymerization dynamics.

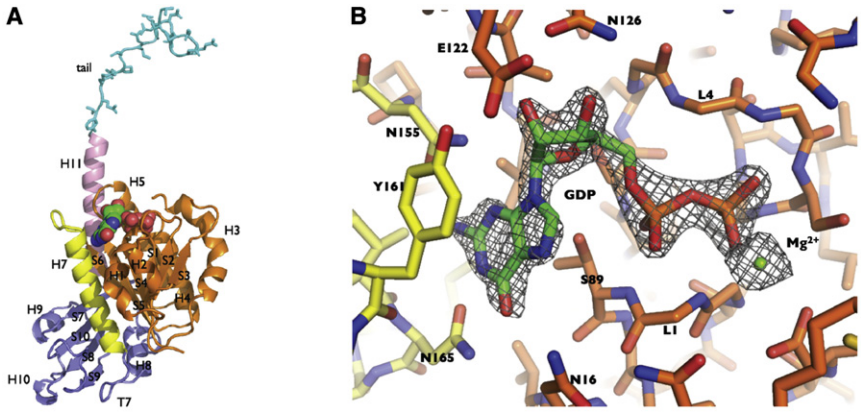

Figure 4. Structure and Nucleotide Binding of PhuZ

(A) Cartoon representation of the PhuZ structure with the N-terminal domain shown in orange, the interdomain in yellow, the C-terminal domain in slate, helix H11 in pink, and the C-terminal tail in cyan is illustrated. The bound GDP is shown as spheres.

(B) Top-down view of the nucleotide-binding pocket. $2F_o$-F_c prior to addition of Mg-GDP to model shown as mesh at 2 σ is demonstrated.

See also Figure S3 and Tables S1 and S2.

PhuZ Forms a Filament in the Crystal with Longitudinal-Spacing-Consistent EM Observations

Figure 5A shows PhuZ surrounded by its four symmetry-related molecules in the crystal, revealing two parallel protofilaments, related by 2_1 crystallographic symmetry. We propose that the intermolecular contacts, especially the longitudinal contacts, observed in the crystal are informative for those made within a PhuZ filament. Like all other tubulin-like proteins, the nucleotide resides at the longitudinal monomer-monomer interface. However, the longitudinal spacing of 47 Å between monomers observed in the crystal lattice is 3–7 Å longer than that of α/β-tubulin (Nogales et al., 1998b), FtsZ (Oliva et al., 2004, 2007), or TubZ (Aylett et al., 2010), resulting in the smallest longitudinal interface seen among tubulins. In PhuZ, terminal side-chain atoms of only ten residues in the longitudinal interface lose solvent accessible surface area due to crystal packing, burying only 188 Å^2/monomer as compared with typical values of 1,666 and 1,034 Å^2 for α/β-tubulin and FtsZ, respectively. Although the gap between monomers is highly solvated, no single water directly contacts the two monomers, and no waters that bridge the two are resolved. This interaction mode is related to, but more extreme than, the one observed for *A. aeolicus* FtsZ, which has a smaller interaction surface than other FtsZs at 655 Å^2 (Oliva et al., 2007). In both of these cases, interactions between the intermediate domain of one monomer and H10 of the other are missing. In PhuZ the residues of the catalytic T7 loop do not appear to be positioned correctly for hydrolysis, with the catalytic Asp side chains being displaced by more than 3 Å from where expected if they were to be able to interact with the γ-phosphate. This is likely a consequence of the structure containing GDP, and there may well be changes in local conformation or monomer packing upon GTP binding.

Unlike eukaryotic tubulins, PhuZ does not make canonical lateral interactions. Instead, each PhuZ is rotated by 180° about an axis parallel to the filament and translated by 23.5 Å, resulting in interdigitated-corner contacts defining a flat ribbon. Although roughly analogous to interactions in TubZ, the TubZ translation is significantly smaller, and the rotation angle is ~190° (Aylett et al., 2010), resulting in a helical filament reminiscent of actin-like polymers. More precisely, the lateral-corner contacts between PhuZ monomers are defined by interactions of H3 on one monomer with H4 and H5 on another (Figure 5A). This interaction occurs twice, so as to interact with two lateral PhuZ monomers. A total surface area of 476 Å^2 per monomer is buried, stabilizing the connection between the two longitudinal protofilaments.

To assess the relevance of the putative filaments formed within the crystal lattice, we compared them more closely with the filaments seen by negative-stain EM (Figure 5C). Two-dimensional averages of 1,000 defined segments were generated to produce a reliable view of monomer packing. Although the filament architecture is not yet clear, the average reveals a PhuZ filament morphology similar to that observed in the crystals. Of particular importance, the longitudinal spacing derived from EM (~45 Å) is consistent with the 47 Å spacing in the crystal, supporting our hypothesis that the crystal lattice provides a suitable model for interactions stabilizing filament formation. This observed spacing is longer than observed for other tubulins, 40–42 Å, and would require a compaction of the lattice in order for the catalytic residues of the T7 loop to come into position for nucleotide hydrolysis. It is possible that the crystal lattice represents an expansion of the filament lattice that would occur after GTP is hydrolyzed to GDP.

The Unique PhuZ C-Terminal Tail Makes Extensive Interactions Required for Polymer Formation

By contrast with the minimal direct longitudinal interface, the 21 C-terminal residues make extensive contacts with the neighboring longitudinal monomer, with a total buried surface area of 1,226 Å^2/monomer. Many of these contacts are driven by either electrostatic or polar interactions (Figure 5B). The 13-most C-terminal residues of the protein contain 6 acidic residues (D303, D305, D306, D309, D311, E310), forming an acidic "knuckle" that is inserted into a basic patch of the longitudinal symmetry mate formed by helices H3, H4, and H5, containing R60, R68, and K135. Nonpolar residues of the knuckle interact with L64, L104, and I140 on the symmetry mate, providing further stabilization. Although the most C-terminal residues make the most extensive contacts, significant interactions are also provided by the extended eight residues that lie between H11 and the knuckle, including significant interactions of R298 with E138, Q297 with Q207, and F295 with I227. These residues,

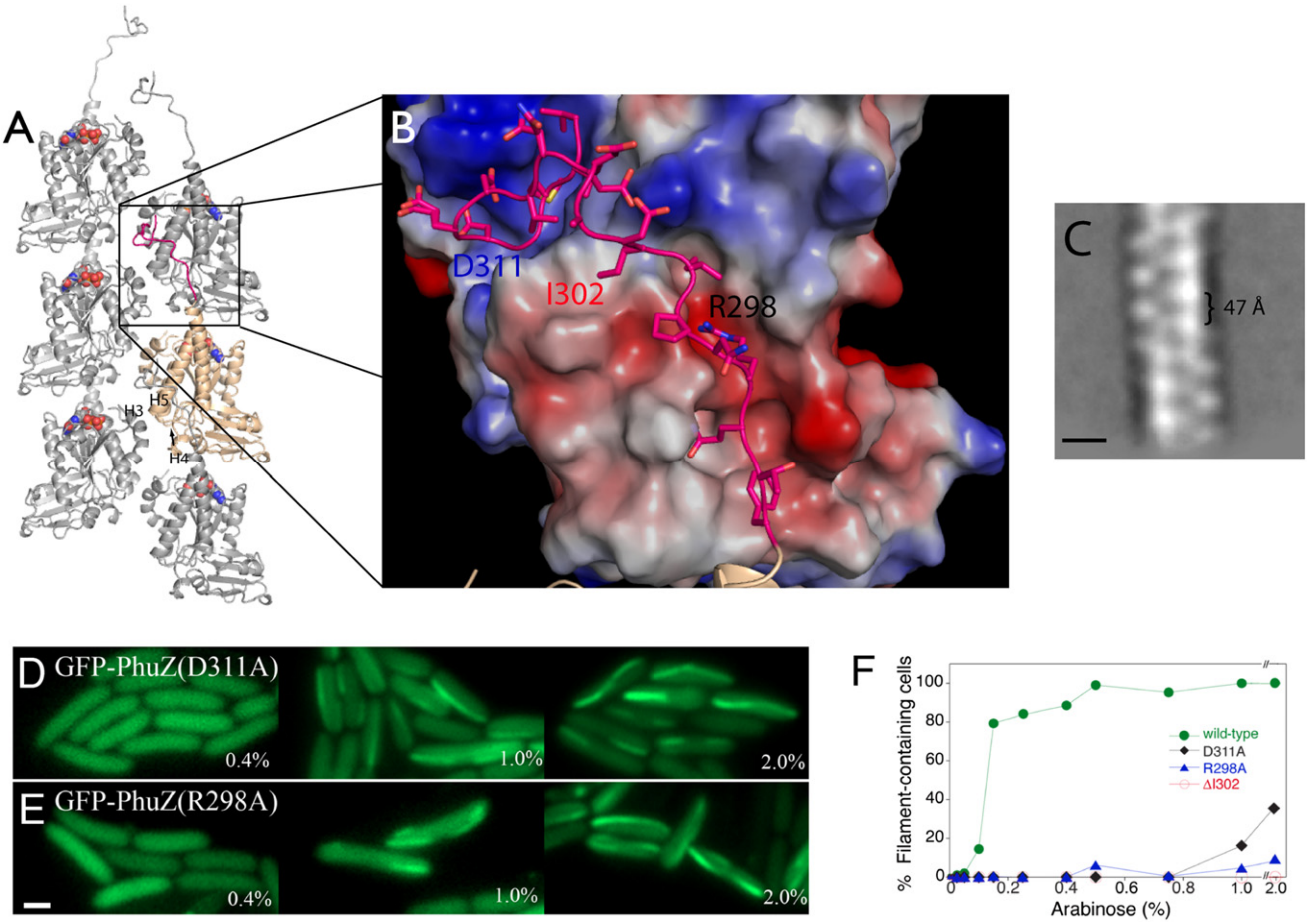

Figure 5. Crystal Lattice Contains Filament-like Contacts with the C-Terminal Tail Providing Most of the Contact Surface

(A) Cartoon representation of PhuZ (wheat with hot-pink tail) with five symmetry mates (grey), nucleotide shown as spheres, reveals two-stranded filament within the crystal lattice and extensive contacts by the C-terminal tail.

(B) A zoomed-in view of the boxed area in (A), showing the electrostatic surface of PhuZ shown interacting with the C-terminal tail. The tail buries 1,226 Å^2 of surface area per monomer. Residues R298, I302, and D311 are highlighted.

(C) Average of 500 segments of PhuZ polymers observed by negative-stain EM is shown. Spacing between longitudinal monomers is ~47 Å. Scale bar, 50 Å.

(D and E) Fluorescent micrographs of *P. chlororaphis* cells expressing the C-terminal tail mutants D311A (D) and R298A (E) grown at room temperature and induced with the indicated amount (%) of arabinose are presented. Both fail to assemble polymers except at the highest expression levels (1% and 2%). Scale bar, 1 μm.

(F) Graph showing the percentage of cells containing filaments when fusion proteins are expressed at increasing levels at 25°C.

See also Figure S4.

especially the aspartic acids of the acid knuckle, are also conserved in the other PhuZ sequences (Figure 1C), suggesting that other phage tubulins may contain a similar C-terminal tail.

Given the extensive interactions contributed by the C-terminal tail, and the otherwise rather limited interactions that stabilize the longitudinal interface, the tail is likely quite important for polymer formation. To test this, we made 2 point mutants (R298A, D311A) to disrupt salt bridges as well as a truncation mutant, ΔI302, that removed the last 13 residues (knuckle region) and examined the functional consequences in vitro by light scattering (Figure 3B). Even at a concentration of 20 μM and in the presence of 1 mM GTP, PhuZ-ΔI302 was unable to form detectable polymer in vitro, whereas wild-type PhuZ polymerizes efficiently at concentrations above 5 μM (Figures 3A and 3B). Similarly, both the R298A and D311A mutants, which disrupt salt bridge and H-bond formation with H5 and H11 and H3, respectively, also compromise in vitro filament formation, with no detectable polymerization at 20 μM (Figure 3B).

These mutants were also tested for their ability to form polymers in vivo by expressing them in *P. chlororaphis*. GFP fusion proteins containing point mutations (D311A and R298A) in the tail were severely impaired for assembly and only formed polymers at the highest expression levels (1% or 2% arabinose, Figures 5D–5F). The C-terminal tail truncation (ΔI302) completely abolished filament formation in vivo at all expression levels (Figure 5F). Using in-gel fluorescence, we demonstrated that all of the C-terminal fusions were stably produced at the expected levels in vivo (Figure S4). These findings demonstrate

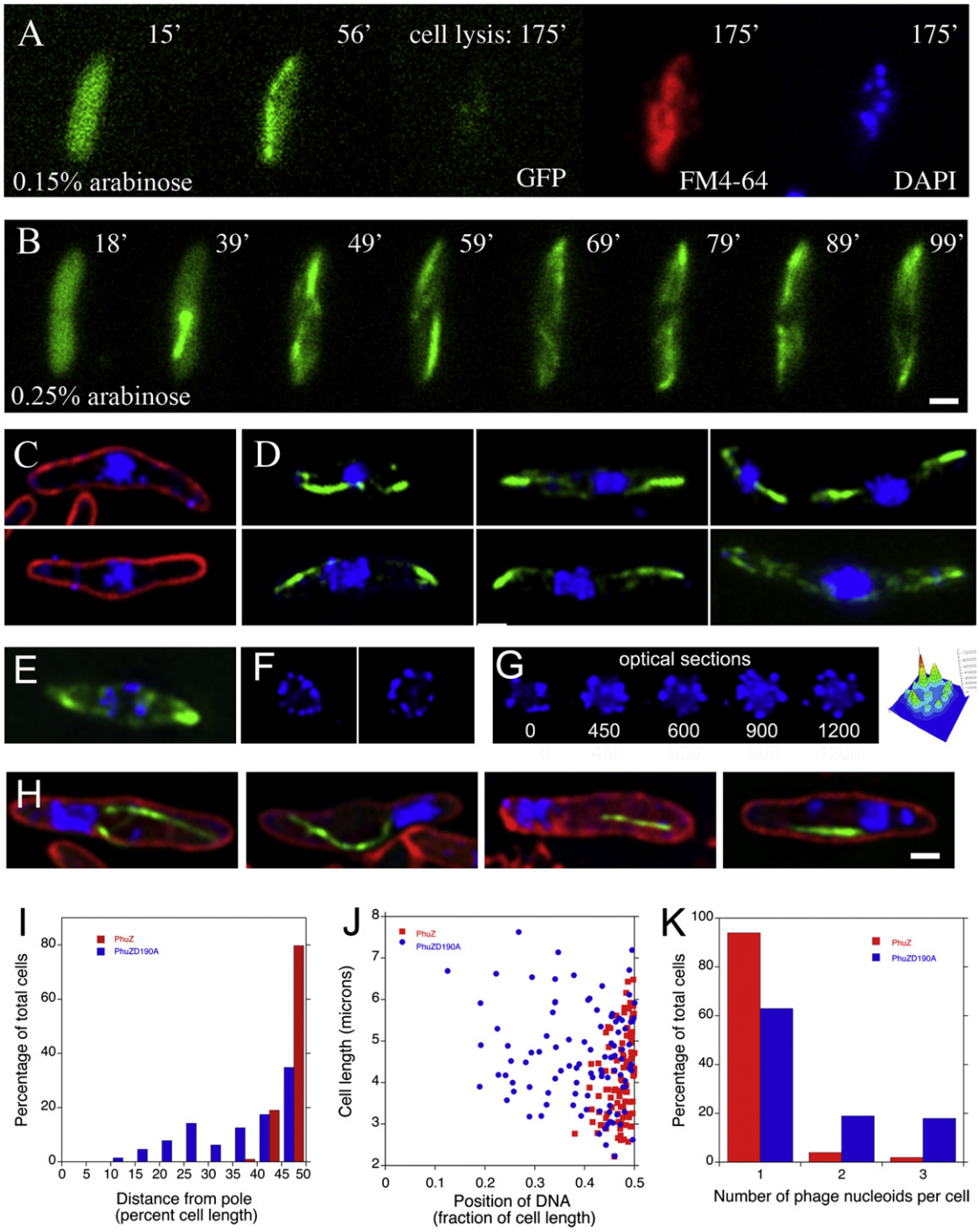

Figure 6. A Single-Cell Assay for Phage Infection Reveals that PhuZ Assembles Filaments In Vivo during Infection of the Host Cell with 201ϕ2-1

(A) In cells grown with 0.15% arabinose (below critical threshold-inducer concentration), filaments first appeared 56 min after phage addition, and the cell lysed after 175 min, as revealed by FM4-64 staining. Staining with DAPI/DNase I indicates phage release.

(B) In cells grown with 0.25% arabinose, filaments first appeared 39 min after phage addition, and polymers underwent cycles of assembly and disassembly until the cell lysed after 140 min. Scale bar, 1 μm.

(C) Two examples of infected cells stained with FM4-64 (red) and DAPI (blue) at 90 min postinfection showing a large mass of DNA in the center of the cell.

(D) Six examples of infected cells showing filaments of GFP-PhuZ on either side of a centrally located DAPI-stained nucleoid.

(E–G) Cells were fixed and treated with DNase I to degrade all DNA except that encapsidated by phage. (E) An example of GFP-PhuZ filaments surrounding DAPI foci at midcell. (F) Two examples of rosette structures formed during infection and visualized after DNase I digestion. (G) A series of optical sections through

the importance of the C-terminal 21 residues of PhuZ in polymerization.

PhuZ Assembles a Dynamic Spindle-like Array during Phage Lytic Growth

One anticipated function for PhuZ is as a DNA segregation system during lysogeny if 201ϕ2-1 replicates separately from the chromosome like a plasmid. Although an attractive hypothesis, so far, we have been unable to obtain lysogens of 201ϕ2-1 in *P. chlororaphis*. Therefore, we sought to determine if PhuZ was expressed and assembled polymers during lytic growth. First, we used RT-PCR to show that *phuZ* mRNA accumulates at 2 hr postinfection (Figure S5A). Second, we devised a microscopic single-cell assay to determine if PhuZ assembles polymers during an infection cycle. To accomplish this, *P. chlororaphis* cells were grown on an agarose pad at 30°C, and GFP-PhuZ was expressed from the arabinose promoter below its critical threshold for assembly (0.15% arabinose at 30°C). We then infected cells with phage and performed time-lapse microscopy in which GFP-PhuZ assembly, phage production, and phage-mediated cell lysis were simultaneously monitored. Because GFP-PhuZ does not spontaneously assemble polymers at this expression level, polymers would only be observed if additional PhuZ (or a regulator of PhuZ assembly) was expressed by the phage. By including DAPI and DNase I in the pad, the release of phage upon cell lysis could be visualized. DNase I degrades any remaining cellular DNA, but not DNA packaged within viral capsids. At the terminal time point, after cells had lysed, we captured images of DAPI fluorescence, allowing the number of released phage particles to be counted. Cell lysis was detected using the membrane dye FM4-64, which only faintly stains wild-type *P. chlororaphis* but intensely stains cell debris.

In the first example (Figure 6A), GFP-PhuZ formed diffuse fluorescence at the beginning of the experiment (15 min after the addition of phage). Within 56 min, GFP-PhuZ assembled a polymer that extended from pole to pole (Figure 6A). This cell maintained at least one polymer for the next 175 min, at which point the cell lysed. DAPI staining alongside DNase I treatment confirmed that this cell had released phage particles, indicating that lysis was phage induced.

In the example shown in Figure 6B, GFP-PhuZ was expressed at a slightly higher level (0.25% arabinose) to allow for brighter images and more frequent time points. At early time points (18 min after phage addition), fluorescence was uniform, but over time, one (39 min) and then multiple (59 min) filaments formed (Figure 6B). Filaments were very dynamic (Figure 6B; Movie S4), undergoing cycles of assembly and disassembly, with at least one filament always assembled until the cell ultimately lysed.

To gain additional insight into the role of PhuZ polymers during lytic growth, we simultaneously visualized GFP-PhuZ and DNA in fixed cells that had been stained with DAPI. During lytic growth, cells became elongated and formed an unusual bulge at the cell midpoint (Figure 6C). DAPI staining revealed that the central bulge contained a high concentration of DNA, which we refer to as the "infection nucleoid," whereas the rest of the cell contained very little DNA (Figure 6C). In comparison, uninfected cells contained one or two vegetative nucleoids that filled the majority of the cytoplasm (Figure S5B). Quantitation showed that most cells contained just a single infection nucleoid (Figure 6K) that was located within 5% of the middle of the cell in 80% of cells and within 10% of the middle in 98% of cells (Figure 6I). PhuZ filaments frequently appeared to make contact with the edge of the infection nucleoid, forming an array on either side of this structure (Figure 6D). Multiple filaments of various lengths (ranging from 0.2 to 2μm) were observed in fixed cells (Figure 6D), as might be expected for a population of cells containing dynamic polymers trapped in various states of polymerization.

To determine if the centrally located DNA masses contained phage-encapsidated DNA, we digested them with DNase I. As shown in the examples in Figures 6E–6G, upon DNase I treatment, much of the centrally located DNA was degraded, leaving DNase I-resistant foci, indicative of phage-encapsidated DNA. PhuZ filaments were extended on each side of these DNA foci (Figure 6E). Optical sectioning revealed that these phage-encapsidated DNA molecules occurred in a rosette-like structure at the edges of the digested nucleoid (Figures 6F and 6G; Movie S5), suggesting that phage DNA occurs in an organized structure at the cell midpoint.

Dynamic Filaments Are Required for Phage Positioning and Maximal Burst Size

Because the majority of phage-infected cells contained PhuZ polymers that extended on each side of the centrally located infection nucleoid, we speculated that PhuZ participates in DNA organization or positioning. To test this idea, we examined DNA positioning in cells expressing either wild-type GFP-PhuZ or a mutant version (GFP-PhuZD190A) that we demonstrated (Figure 2) assembles static polymers in vivo. In other tubulins, including TubZ (Larsen et al., 2007) and FtsZ (Lu et al., 2001), catalytic mutants defective in GTP hydrolysis coassemble with

a DNase I-digested nucleoid showing that phage-encapsidated DNA occurs in a circular pattern. Numbers indicate distance in nanometers from the first optical section. On the far right is a 3D fluorescence intensity graph of DAPI fluorescence corresponding to the 900 nm optical section showing the rosette pattern of foci localization.

(H) Four panels showing DAPI-stained cells expressing the GTPase mutant GFP-PhuZD190A after 90 min of phage infection. The phage nucleoid is frequently positioned at the pole of the cell. Some cells (far left) contain two or three nucleoids. Scale bar, 1 μm.

(I) Histogram showing the percentage of cells with the phage nucleoid located near the center (50% cell length) of the cell for wild-type GFP-PhuZ (red) or mutant GFP-PhuZD190A (blue).

(J) Graph showing the position of the phage nucleoid as a fraction of cell length versus cell length for wild-type GFP-PhuZ (red) or mutant GFP-PhuZD190A (blue).

(K) Histogram showing the percentage of infected cells expressing either wild-type GFP-PhuZ (red) or mutant GFP-PhuZD190A (blue) containing one, two, or three phage nucleoids.

See also Figure S5 and Movies S4, S5, and S6.

the wild-type and behave as dominant negatives. Positioning of the nucleoid during infection was severely affected by expression of GFP-PhuZD190A; only 39% of mutant cells positioned the infection nucleoid within 5% of the middle (compared to 80% for wild-type; Figure 6I). In many cells, the PhuZD190A filaments appeared to make contact with the edge of an infection nucleoid that was mispositioned close to the cell pole (Figure 6H). Significant mispositioning occurred in the mutant cells regardless of their size (Figure 6J). In addition whereas 94% of cells infected in the presence of wild-type PhuZ had a single large nucleoid, more than one-third of infected cells expressing PhuZD190A contained either two or three nucleoids (Figures 6H and 6 K), typically present at random positions, further indicating disruption of DNA localization. Taken together, these results suggest that PhuZ assembles a dynamic cytoskeletal element that functions to position phage at the cell midpoint during phage lytic growth.

To assess the importance of PhuZ to phage yield, we attempted population-based phage growth curves, but phage infections rates were too low to make the results interpretable. We therefore performed single-cell infection assays and found a significant decrease in burst size when cells expressed the PhuZD190A catalytic mutant, from an average of 16 phage per cell for wild-type ($n = 25$) to an average of 7 ($n = 25$) for the mutant ($p = 0.0001$). Proper phage centering by PhuZ thus contributes significantly to the efficiency of phage production. Such a 50% reduction in yield would be a significant evolutionary disadvantage.

DISCUSSION

Identification of a Prokaryotic DNA-Positioning "Spindle"

Here, we describe a phage-encoded spindle-like array assembled from a distant relative of tubulin. No phage-encoded actin or tubulin cytoskeletal element has been previously characterized, and therefore, the function of this protein was unclear. Because many phage replicate as plasmids during lysogenic growth, we initially suspected that the function and polymerization properties of PhuZ might be similar to those of the *Bacillus thuringiensis* plasmid segregation protein TubZ. Surprisingly, we found that PhuZ has a structure unlike any other tubulin and a function that provides new paradigms for understanding the mechanism of tubulin polymerization and its cellular activity. We show that the C-terminal tail of PhuZ drives polymerization of a dynamic filament that positions phage DNA within the center of the cell, demonstrating that a prokaryotic cytoskeleton can perform a function analogous to the microtubule-based spindle that positions chromosomes on the metaphase plate or tubulin cytoskeletal elements that position nuclei (Tran et al., 2001) in eukaryotes.

Unique Features of the PhuZ Monomer Define Polymer Contacts

Although the overall fold of PhuZ is tubulin like, the structure of the monomer possesses key differences from tubulin/FtsZ/TubZ family members, leading to a unique filament organization. Whereas the C-terminal extensions of other tubulins are known to be important interaction sites for accessory proteins that modulate polymer state, or otherwise affect function (e.g., microtubule-associated proteins [MAPs], FtsA, MinC, TubR), our results reveal that the PhuZ C terminus has uniquely evolved a critical role in polymer formation, providing the vast majority of the buried surface area that stabilizes filament formation.

The other striking feature of PhuZ is the lack of helix H6. In other tubulins, the conserved H6 provides a surface for key longitudinal interactions between monomers. Lack of this helix in PhuZ leaves a large open surface on what we believe to be the outside of the polymer. In α/β-tubulin, a concerted movement of helices 6 and 7 is key to the transition between the curved and straight conformations, which affects both the ease of incorporation into the growing microtubule lattice and the degree of metastability once GTP hydrolyzes. Although it is unclear if motion of H7 is relevant to PhuZ function, it is intriguing to speculate that the acidic pocket created by the loss of H6 could serve as a binding surface for interacting proteins, thereby coupling the binding to altered polymer dynamics.

The structure provides few clues as to how nucleotide controls PhuZ polymerization, though it suggests that it polymerizes through an atypical mechanism for a tubulin family member. There is no indication that the C-terminal tail interactions, which dominate longitudinal association, are in any way modulated by nucleotide. The disordered L3 loop (residues 55–57) near where the γ-phosphate should bind may very well become ordered by GTP binding but seems too distant from the next monomer to directly affect polymerization. It is quite possible that PhuZ undergoes a nucleotide-dependent conformational change, like that seen for TubZ. An interesting possibility for PhuZ is that the lattice might compact longitudinally with GTP, both enhancing "classical" longitudinal interactions and bringing the catalytic residues into proximity for hydrolysis. Thus, the potential of the C-terminal tail to provide a unique degree of flexibility in the longitudinal interface may be an important feature of the PhuZ polymer required for in vivo function and the control of its dynamics. Ultimately, it will be necessary to solve structures of PhuZ bound to other nucleotides, as well as in a nonpolymer state, to gain mechanistic insight into the role of nucleotide binding and hydrolysis in polymer formation and dynamics.

Conservation of the PhuZ Polymerization Mechanism

The C-terminal tail of PhuZ is conserved among a number of prokaryotic tubulins, including a set of *Clostridium* proteins (Figure 1C), which are otherwise highly divergent in sequence, suggesting that this mechanism of polymerization is not restricted to *Pseudomonas* phage. Among three *Pseudomonas* phage proteins and four *Clostridial* phage proteins, the acidic knuckle, the hydrophobic amino acids, and R298 are all conserved. Some of the amino acids that interact with the tail are also conserved, such as R60, which is conserved in all seven of these proteins. E138, which makes a salt bridge with R298, is also conserved among the *Pseudomonas* proteins, and although the *Clostridial* proteins lack E138, they contain a conserved aspartic acid residue nearby that could complete the salt bridge. Intriguingly, residues D303, D305, and D306 are highly conserved among these seven proteins, even though they all

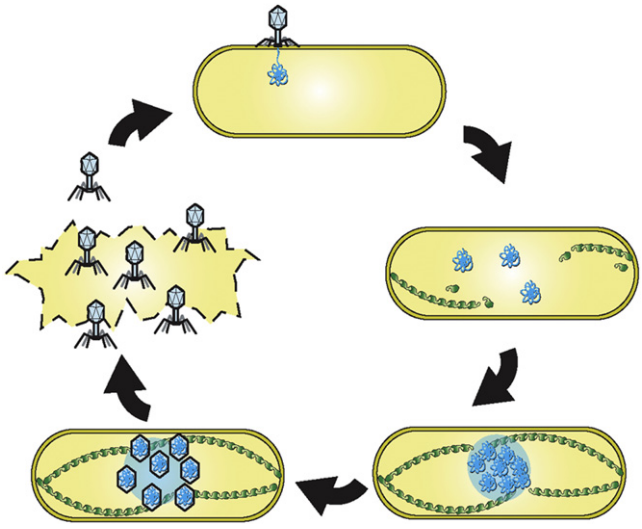

Figure 7. Model for the Role of PhuZ Filaments in the 201ϕ2-1 Phage Cycle

After 201ϕ2-1 infects a cell, the host chromosome is degraded, and short PhuZ filaments appear that eventually extend from the poles of the cell to the phage nucleoid in the center. The PhuZ spindle positions the phage DNA in the center of the cell to allow 201ϕ2-1 genomes to be efficiently replicated and/or packaged into the capsids. After the completion of phage assembly, the cell lyses, expelling mature phage into the environment.

point out into the solvent in the structure, suggesting that they may be conserved for other protein-protein interactions. Curiously, GP16 of *Pseudomonas* phage EL is missing the conserved C-terminal tail amino acids (R298 and the IIDIDD motif), the corresponding salt bridge residues (R60 and E138), and contains multiple substitutions in the highly conserved G box, suggesting that its mechanism of polymerization has diverged.

PhuZ Controls Positioning of Phage DNA

PhuZ represents, to our knowledge, the first characterized tubulin cytoskeletal element encoded by a phage. PhuZ assembles a dynamic array that positions phage DNA at the center of the cell. How might a tubulin polymer position phage DNA? We recently demonstrated that dynamically unstable polymers can center DNA in a bacterial cell by constantly applying pushing forces that readjust its position relative to the poles of the cell (Drew and Pogliano, 2011), much like *S. pombe* nuclei are positioned by pushing of interphase microtubule arrays (Tran et al., 2001). We therefore speculate that PhuZ forms dynamically unstable polymers capable of exerting pushing forces that position phage DNA at midcell (Figure 7). Consistent with this model, during phage infection GFP-PhuZ formed highly dynamic polymers that appeared to undergo many cycles of assembly and disassembly. Altering the polymerization dynamics of PhuZ filaments by expressing a catalytic mutant strongly disrupted DNA positioning, showing that dynamic assembly is important for its centering activity. Coupling of the pushing force to the DNA likely involves one or more adaptor proteins that interact with one end of the PhuZ polymer and also with either phage DNA or proteins involved in phage replication and/or capsid assembly.

What is the advantage of positioning phage 201ϕ2-1 DNA in the cell center? Many eukaryotic viruses replicate in a specific region of the cell, including in the cytosol, the nucleoplasm, or in tight association with specific intracellular membrane compartments (Leopold and Pfister, 2006; Radtke et al., 2006). Concentrated zones of viral replication (often referred to as factories) likely increase the efficiency of viral replication and assembly. Gamma herpes virus, for example, forms replication factories surrounded by newly assembled viral particles (Iwasaki and Omura, 2010). We show here that encapsidated 201ϕ2-1 DNA occurs at midcell in a rosette-like structure surrounding a larger DNA mass, suggestive of the formation of a viral factory. Expression of the catalytic mutant decreased phage yield by 50%, indicating that dynamic PhuZ filaments improve the overall efficiency of phage production. We speculate that localization of phage DNA at midcell might facilitate replication, phage assembly, or phage release, although we currently cannot distinguish between these possibilities. For example, keeping phage DNA concentrated in the center may facilitate efficient packaging into capsids and be especially important for very large genomes where movement by diffusion would be severely limited. Consistent with this idea, all of the tubulin-encoding phage that we have so far identified are very large, with genomes ranging in size from 185 (Sakaguchi et al., 2005) to 316 kb (Thomas et al., 2008). Although midcell localization of phage DNA might also be related to the formation of the central bulge, we note that in mutants in which phage DNA is mispositioned near the cell pole, a bulge still forms in the cell center (Figure 6H), demonstrating that the DNA itself is not responsible for the bulge. Instead, phage DNA may be positioned near the center to take advantage of other important events that might be associated with the bulge, such as capsid production or cell lysis. These results suggest that, as for eukaryotic viruses, large bacterial viruses also benefit from localization to discrete regions of the cell.

Cytoskeletal Proteins Are Widespread among Bacterial Viruses

We have identified at least seven different phage that encode a tubulin-like gene, suggesting that the function of PhuZ may be conserved among very large phage. Previous work has shown that MreB is important for DNA replication of several phage in *E. coli* and *B. subtilis* (Muñoz-Espín et al., 2009). We recently described Alp6A, an actin-like protein encoded by *Bacillus thuringiensis* phage 0305ϕ8-36, that forms polymers of unknown function (Derman et al., 2009). These results suggest that some phage have evolved to use a host cytoskeletal protein (MreB), whereas other, larger phage may have evolved their own specialized cytoskeletal element (PhuZ and Alp6A). Understanding divergent tubulins like PhuZ may provide broader insight into the functions and mechanisms underlying the bacterial tubulin cytoskeleton.

EXPERIMENTAL PROCEDURES

Protein Expression and Purification

The PhuZ gene was cloned into the pET28a expression vector with a 6-His tag on the N terminus and expressed in BL21(DE3) cells under an IPTG-inducible

T7 promoter. PhuZ was purified by Ni-affinity chromatography followed by gel filtration (Superdex 200). For additional details, please see Extended Experimental Procedures.

Crystallization, Structure Determination, and EM

Crystals were grown by the hanging-drop, vapor diffusion method in 2 μl drops containing 1 μl of concentrated protein (2 mg/ml) and 1 μl of precipitant solution (15% PEG 6000, 0.1 M HEPES [pH 7.5], 0.5 M ammonium acetate, 0.05 M $MgCl_2$). Protein structure was determined as described in the Extended Experimental Procedures. Electron micrographs were obtained with a Tecnai T12 microscope at a voltage of 120kV at a magnification of ×52,000. Images were recorded with a Gatan 4k × 4k charge-coupled device camera. For additional details please see Extended Experimental Procedures.

Light Scattering

Right-angle light scattering was conducted by mixing PhuZ with a polymerization buffer containing GTP using a stop-flow system designed in house. An excitation wavelength of 530 nm was used. The critical concentration was determined by plotting the maximum intensity versus PhuZ concentration. The x intercept of this plot was used as the critical concentration.

Strains, Media, and Growth Conditions

P. chlororaphis strain 200-B was grown on the following media: 10 g Bacto Tryptone, 5 g NaCl, in 1,000 ml of dH_2O (Serwer et al., 2004). Plasmids were introduced into *P. chlororaphis* by electroporation (Howard et al., 2007). Lysates of 201ϕ2-1 were made by adding 50 μl of a high-titer lysate (10^9 pfu/ml) to exponentially growing *P. chlororaphis*, shaking at 30°C and incubating for 6 hr. Lysates were clarified by centrifugation at 16,000 rpm and stored at 4°C with chloroform.

Microscopy

P. chlororaphis cells were grown on 1.2% agarose pads containing 25% Luria Broth, 15 μg/ml gentamycin sulfate, 1 μg/ml FM4-64 (Pogliano et al., 1999), and 0, 0.15%, 0.25%, 0.40%, 0.50%, 0.75%, 1.0%, or 2.0% arabinose. The slides were then incubated for 3 hr at either room temperature or 30°C. The cells were imaged with a DeltaVision Spectris Deconvolution microscope (Applied Precision, Issaquah, WA, USA). For FRAP experiments please see Extended Experimental Procedures.

Single-Cell Phage Replication Assays

P. chlororaphis cells were inoculated on a 1.2% agarose pad containing 1/4× Luria Broth, 15 μg/ml gentamycin sulfate, 1 μg/ml FM4-64 (Pogliano et al., 1999), 1 μg/ml DAPI, and either 0.15% or 0.25% arabinose, and incubated at 30°C for 2–4 hr without a coverslip in a humidified box. At time zero, 3 μl of high-titer lysate and 3 μl of 1 mg/ml DNase I (New England BioLabs) were added on top of the cells, and then images were taken every 5–10 min for 180 min. To image DAPI and GFP-PhuZ polymers during infection, cells were fixed as described in Extended Experimental Procedures.

Plasmid Constructions and In-Gel Fluorescence Assays

Plasmids were constructed as described in the Extended Experimental Procedures. GFP-PhuZ expression was examined using in-gel fluorescence as described in the Extended Experimental Procedures.

SUPPLEMENTAL INFORMATION

Supplemental Information includes Extended Experimental Procedures, five figures, two tables, and five movies and can be found with this article online at doi:10.1016/j.cell.2012.04.034.

ACKNOWLEDGMENTS

We thank Justin Farlow for help with early experiments, Dr. Justin Kollman for EM advice, and Jessica Polka for many helpful discussions. We also thank Drs. Julie Thomas and Steven Hardies of UT Health Sciences San Antonio for the 201ϕ2-1 phage and Dr. Hongwei D Yu of Marshall University for the pHERD30T vector. This work was funded by HHMI and NIH Grant GM031627 (to D.A.A.) and by NIH Grants GM084334 and GM073898 (to J.P.). J.A.K. is supported by a Genentech predoctoral fellowship.

Received: December 15, 2011
Revised: February 27, 2012
Accepted: April 13, 2012
Published: June 21, 2012

REFERENCES

Anand, S.P., Akhtar, P., Tinsley, E., Watkins, S.C., and Khan, S.A. (2008). GTP-dependent polymerization of the tubulin-like RepX replication protein encoded by the pXO1 plasmid of *Bacillus anthracis*. Mol. Microbiol. *67*, 881–890.

Aylett, C.H., Wang, Q., Michie, K.A., Amos, L.A., and Löwe, J. (2010). Filament structure of bacterial tubulin homologue TubZ. Proc. Natl. Acad. Sci. USA *107*, 19766–19771.

Becker, E., Herrera, N.C., Gunderson, F.Q., Derman, A.I., Dance, A.L., Sims, J., Larsen, R.A., and Pogliano, J. (2006). DNA segregation by the bacterial actin AlfA during *Bacillus subtilis* growth and development. EMBO J. *25*, 5919–5931.

Cabeen, M.T., and Jacobs-Wagner, C. (2010). The bacterial cytoskeleton. Annu. Rev. Genet. *44*, 365–392.

Chen, Y., and Erickson, H.P. (2008). In vitro assembly studies of FtsZ/tubulin-like proteins (TubZ) from *Bacillus* plasmids: evidence for a capping mechanism. J. Biol. Chem. *283*, 8102–8109.

de Boer, P.A. (2010). Advances in understanding *E. coli* cell fission. Curr. Opin. Microbiol. *13*, 730–737.

Derman, A.I., Becker, E.C., Truong, B.D., Fujioka, A., Tucey, T.M., Erb, M.L., Patterson, P.C., and Pogliano, J. (2009). Phylogenetic analysis identifies many uncharacterized actin-like proteins (Alps) in bacteria: regulated polymerization, dynamic instability and treadmilling in Alp7A. Mol. Microbiol. *73*, 534–552.

Downing, K.H., and Nogales, E. (1998). Tubulin and microtubule structure. Curr. Opin. Cell Biol. *10*, 16–22.

Drew, K.R., and Pogliano, J. (2011). Dynamic instability-driven centering/segregating mechanism in bacteria. Proc. Natl. Acad. Sci. USA *108*, 11075–11080.

Howard, G.T., Mackie, R.I., Cann, I.K., Ohene-Adjei, S., Aboudehen, K.S., Duos, B.G., and Childers, G.W. (2007). Effect of insertional mutations in the pueA and pueB genes encoding two polyurethanases in *Pseudomonas chlororaphis* contained within a gene cluster. J. Appl. Microbiol. *103*, 2074–2083.

Iwasaki, K., and Omura, T. (2010). Electron tomography of the supramolecular structure of virus-infected cells. Curr. Opin. Struct. Biol. *20*, 632–639.

Larsen, R.A., Cusumano, C., Fujioka, A., Lim-Fong, G., Patterson, P., and Pogliano, J. (2007). Treadmilling of a prokaryotic tubulin-like protein, TubZ, required for plasmid stability in *Bacillus thuringiensis*. Genes Dev. *21*, 1340–1352.

Leopold, P.L., and Pfister, K.K. (2006). Viral strategies for intracellular trafficking: motors and microtubules. Traffic *7*, 516–523.

Löwe, J., and Amos, L.A. (1998). Crystal structure of the bacterial cell-division protein FtsZ. Nature *391*, 203–206.

Löwe, J., and Amos, L.A. (2009). Evolution of cytomotive filaments: the cytoskeleton from prokaryotes to eukaryotes. Int. J. Biochem. Cell Biol. *41*, 323–329.

Lu, C., Stricker, J., and Erickson, H.P. (2001). Site-specific mutations of FtsZ—effects on GTPase and in vitro assembly. BMC Microbiol. *1*, 7.

Lutkenhaus, J. (2007). Assembly dynamics of the bacterial MinCDE system and spatial regulation of the Z ring. Annu. Rev. Biochem. *76*, 539–562.

Margolin, W. (2009). Sculpting the bacterial cell. Curr. Biol. *19*, R812–R822.

Michie, K.A., and Löwe, J. (2006). Dynamic filaments of the bacterial cytoskeleton. Annu. Rev. Biochem. *75*, 467–492.

Muñoz-Espín, D., Daniel, R., Kawai, Y., Carballido-López, R., Castilla-Llorente, V., Errington, J., Meijer, W.J.J., and Salas, M. (2009). The actin-like MreB cytoskeleton organizes viral DNA replication in bacteria. Proc. Natl. Acad. Sci. USA *106*, 13347–13352.

Ni, L., Xu, W., Kumaraswami, M., and Schumacher, M.A. (2010). Plasmid protein TubR uses a distinct mode of HTH-DNA binding and recruits the prokaryotic tubulin homolog TubZ to effect DNA partition. Proc. Natl. Acad. Sci. USA *107*, 11763–11768.

Nogales, E., Downing, K.H., Amos, L.A., and Löwe, J. (1998a). Tubulin and FtsZ form a distinct family of GTPases. Nat. Struct. Biol. *5*, 451–458.

Nogales, E., Wolf, S.G., and Downing, K.H. (1998b). Structure of the alpha beta tubulin dimer by electron crystallography. Nature *391*, 199–203.

Oliva, M.A., Cordell, S.C., and Löwe, J. (2004). Structural insights into FtsZ protofilament formation. Nat. Struct. Mol. Biol. *11*, 1243–1250.

Oliva, M.A., Trambaiolo, D., and Löwe, J. (2007). Structural insights into the conformational variability of FtsZ. J. Mol. Biol. *373*, 1229–1242.

Pogliano, J., Osborne, N., Sharp, M.D., Abanes-De Mello, A., Perez, A., Sun, Y.L., and Pogliano, K. (1999). A vital stain for studying membrane dynamics in bacteria: a novel mechanism controlling septation during *Bacillus subtilis* sporulation. Mol. Microbiol. *31*, 1149–1159.

Polka, J.K., Kollman, J.M., Agard, D.A., and Mullins, R.D. (2009). The structure and assembly dynamics of plasmid actin AlfA imply a novel mechanism of DNA segregation. J. Bacteriol. *191*, 6219–6230.

Popp, D., Xu, W., Narita, A., Brzoska, A.J., Skurray, R.A., Firth, N., Ghoshdastider, U., Maéda, Y., Robinson, R.C., and Schumacher, M.A. (2010). Structure and filament dynamics of the pSK41 actin-like ParM protein: implications for plasmid DNA segregation. J. Biol. Chem. *285*, 10130–10140.

Qiu, D., Damron, F.H., Mima, T., Schweizer, H.P., and Yu, H.D. (2008). PBAD-based shuttle vectors for functional analysis of toxic and highly regulated genes in *Pseudomonas* and *Burkholderia* spp. and other bacteria. Appl. Environ. Microbiol. *74*, 7422–7426.

Radtke, K., Döhner, K., and Sodeik, B. (2006). Viral interactions with the cytoskeleton: a hitchhiker's guide to the cell. Cell. Microbiol. *8*, 387–400.

Rivera, C.R., Kollman, J.M., Polka, J.K., Agard, D.A., and Mullins, R.D. (2011). Architecture and assembly of a divergent member of the ParM family of bacterial actin-like proteins. J. Biol. Chem. *286*, 14282–14290.

Sakaguchi, Y., Hayashi, T., Kurokawa, K., Nakayama, K., Oshima, K., Fujinaga, Y., Ohnishi, M., Ohtsubo, E., Hattori, M., and Oguma, K. (2005). The genome sequence of *Clostridium botulinum* type C neurotoxin-converting phage and the molecular mechanisms of unstable lysogeny. Proc. Natl. Acad. Sci. USA *102*, 17472–17477.

Schlieper, D., Oliva, M.A., Andreu, J.M., and Löwe, J. (2005). Structure of bacterial tubulin BtubA/B: evidence for horizontal gene transfer. Proc. Natl. Acad. Sci. USA *102*, 9170–9175.

Serwer, P., Hayes, S.J., Zaman, S., Lieman, K., Rolando, M., and Hardies, S.C. (2004). Improved isolation of undersampled bacteriophages: finding of distant terminase genes. Virology *329*, 412–424.

Sontag, C.A., Staley, J.T., and Erickson, H.P. (2005). In vitro assembly and GTP hydrolysis by bacterial tubulins BtubA and BtubB. J. Cell Biol. *169*, 233–238.

Thanbichler, M., and Shapiro, L. (2008). Getting organized—how bacterial cells move proteins and DNA. Nat. Rev. Microbiol. *6*, 28–40.

Thomas, J.A., Rolando, M.R., Carroll, C.A., Shen, P.S., Belnap, D.M., Weintraub, S.T., Serwer, P., and Hardies, S.C. (2008). Characterization of *Pseudomonas chlororaphis* myovirus 201varphi2-1 via genomic sequencing, mass spectrometry, and electron microscopy. Virology *376*, 330–338.

Tran, P.T., Marsh, L., Doye, V., Inoué, S., and Chang, F. (2001). A mechanism for nuclear positioning in fission yeast based on microtubule pushing. J. Cell Biol. *153*, 397–411.

van den Ent, F., Amos, L.A., and Löwe, J. (2001). Prokaryotic origin of the actin cytoskeleton. Nature *413*, 39–44.

Note Added in Proof

While this paper was in press, the structure of another bacteriophage-encoded tubulin from a divergent class (Cst in Figure 1, above) was published by Olivia et al. By contrast with PhuZ, Olivia et al. propose that Cst phage TubZ is involved in plasmid segregation during lysogeny. Oliva, M.A., Martin-Galiano, A.J., Sakaguchi, Y., and Andreu, J.M. (2012). Tubulin homolog TubZ in a phage-encoded partition system. Proc. Natl. Acad. Sci. USA *109*, 7711–7716.